

Mol #113076

The novel activity of carbamazepine as an activation modulator extends from Nav1.7 mutations to the Nav1.8-S242T mutant channel from a patient with painful diabetic neuropathy

Chongyang Han, Andreas C. Themistocleous, Mark Estacion, Fadia B. Dib-Hajj, Iulia Blesneac, Lawrence Macala, Carl Fratter, David L. Bennett, Stephen G. Waxman, Sulayman D. Dib-Hajj

Department of Neurology and Center for Neuroscience and Regeneration Research Yale University School of Medicine, New Haven, CT 06510, USA; Center for restoration of Nervous System Function, Veterans Affairs Medical Center, West Haven, CT 06516, USA
(C.H., M.E., F.B.D-H., L.M., S.G.W., S.D.D-H)

Nuffield Department of Clinical Neurosciences, University of Oxford, Oxford, UK
(A.C.T., I.B., D.L.B)

Brain Function Research Group, School of Physiology, Faculty of Health Sciences, University of the Witwatersrand, Johannesburg, South Africa
(A.C.T)

Oxford Medical Genetics Laboratories, Oxford University Hospitals NHS Foundation Trust, Oxford, UK.
(C.F)

Mol #113076

Running title: Carbamazepine-responsive Nav1.8 mutation

Corresponding author:

Sulayman D. Dib-Hajj, PhD

The Center for Neuroscience and Regeneration Research

VA Connecticut Healthcare System

950 Campbell Avenue, Bldg. 34

West Haven, CT 06516

Tel: (203)937-3802

Fax: (203)937-3801

E-mail: Sulayman.dib-hajj@yale.edu

Number of text pages: 41

Number of figures: 7

Number of references: 49

Abstract: 221 Words

Introduction: 721 Words

Discussion: 1500 Words

Abbreviations: voltage-gated sodium channel (Nav); dorsal root ganglion (DRG); carbamazepine (CBZ); intra-epidermal nerve fiber density (IENFD); Quantitative sensory testing (QST); Toronto Clinical Scoring System (TCSS); The Douleur Neuropathique 4 Questionnaire (DN4); dimethylsulfoxide (DMSO); Molecular Operating Environment (MOE); minimal allele frequency (MAF); inherited erythromelalgia (IEM); diabetic peripheral neuropathy (DPN)

Mol #113076

Abstract

Neuropathic pain in patients carrying sodium channel gain-of-function mutations is generally refractory to pharmacotherapy. However, we have shown that pre-treatment of cells with clinically-achievable concentration of carbamazepine (CBZ, 30 μ M) depolarizes voltage-dependence of activation in some Nav1.7 mutations such as S241T, a novel CBZ mode-of-action of this drug. CBZ reduces the excitability of dorsal root ganglion (DRG) neurons expressing Nav1.7-S241T mutant channels, and individuals carrying the S241T mutation respond to treatment with CBZ. Whether the novel activation-modulating activity of CBZ is specific to Nav1.7, and whether this pharmacogenomic approach can be extended to other sodium channel subtypes, are not known. We report here the novel Nav1.8-S242T mutation, which corresponds to the Nav1.7-S241T mutation, in a patient with neuropathic pain and diabetic peripheral neuropathy. Voltage-clamp recordings demonstrated hyperpolarized and accelerated activation of Nav1.8-S242T. Current-clamp recordings showed that Nav1.8-S242T channels render DRG neurons hyperexcitable. Structural modeling shows that despite substantial difference in the primary amino acid sequence of Nav1.7 and Nav1.8, the S242 (Nav1.8) and S241 (Nav1.7) residues have similar position and orientation in the domain I S4-S5 linker of the channel. Pretreatment with a clinically-achievable concentration of CBZ corrected voltage-dependence of activation of Nav1.8-S242T channels, and reduced DRG neuron excitability as predicted from our pharmacogenomic model. These findings extend the novel activation-modulation mode-of-action of CBZ to a second sodium channel subtype, Nav1.8.

Mol #113076

Introduction

Sodium channels underlie the initiation and propagation of action potentials, and gain-of-function mutations of sodium channels have been linked to a spectrum of human pain disorders (Bennett and Woods, 2014; Dib-Hajj et al., 2015; Dib-Hajj et al., 2010; Dib-Hajj et al., 2017). The Nav1.8-tetrodotoxin-resistant (TTX-R) sodium channel is preferentially expressed in dorsal root ganglion (DRG) neurons (Akopian et al., 1996), has been shown to contribute most of the sodium current underlying the rising phase of action potentials (Blair and Bean, 2002; Renganathan et al., 2001), and supports high-frequency firing in response to depolarization (Renganathan et al., 2001). Nav1.8 has been linked to pain in a rat model of diabetes (Mert and Gunes, 2012). Electrophysiological recordings have shown increased TTX-R sodium currents from small-diameter DRG neurons from diabetic rats, accompanied by shifts in voltage-dependence of activation and steady-state fast-inactivation of the channel (Hong et al., 2004). Exposure of DRG neurons to methylglyoxal, a glucose metabolite that accumulates in diabetes, has been shown to depolarize voltage-dependence of fast-inactivation of Nav1.8 and produce a reduction in rheobase, consistent with a contribution of Nav1.8 to hyperexcitability of these neurons in diabetic models (Bierhaus et al., 2012). Recently, gain-of-function Nav1.8 mutations have been identified in patients with painful small fiber neuropathy (SFN), including subjects with diabetic peripheral neuropathy (DPN) (Faber et al., 2012b; Han et al., 2014; Huang et al., 2013).

Although carbamazepine (CBZ), an FDA-approved antiepileptic Navs blocker, is not recommended as a first line treatment for neuropathic pain (Finnerup et al., 2015), it is still used clinically in selected patients with some success. Importantly, CBZ has demonstrated effectiveness in treatment for the pain disorder trigeminal neuralgia (Maarbjerger et al., 2017). The

Mol #113076

classical action of CBZ is to inhibit Navs in a voltage- and use-dependent manner (Kuo, 1998; Kuo et al., 1997; Tanelian and Brose, 1991; Yang et al., 2010). Although CBZ action on VGSC is indisputable, especially at clinically-achievable concentrations, it has been shown to also act on other ion channels and receptors (Ambrosio et al., 2002) that might contribute to its analgesic effect. Recently, we have demonstrated a novel action of CBZ as an activation modulator of mutant Nav1.7 channels, in which clinically-achievable concentrations of CBZ (10-30 μ M) depolarize voltage-dependence of activation; plasma levels in patients with epilepsy treated with CBZ range from 0.92-16 mg/L, which correspond to 3.89-67.5 μ M (Breton et al., 2005). CBZ (10-30 μ M) depolarize activation of mutant Nav1.7 channels including Nav1.7-S241T (Yang et al., 2012), Nav1.7-V400M (Fischer et al., 2009) and Nav1.7-I234T (Yang et al., 2017), but not wild-type Nav1.7, and reduces excitability of DRG neurons that express these mutant Nav1.7 channels (Geha et al., 2016; Yang et al., 2017; Yang et al., 2012). Open label use of CBZ was reported to be beneficial in treating IEM patients carrying the Nav1.7-V400M mutation (Fischer et al., 2009) and Nav1.7-I234T mutation (Meijer et al., 2014). In a placebo controlled, double-blind clinical study, we showed that CBZ (plasma concentration of 3.6-6.0 mg/L, which corresponds to 15.22-25.37 μ M) was effective in treating patients with inherited erythromelalgia (IEM) carrying the Nav1.7-S241T mutation (Geha et al., 2016). However, except for the pharmacogenomic targeting of Nav1.7 carrying specific CBZ-responsive mutations (Fertleman et al., 2006; Fischer et al., 2009; Geha et al., 2016; Meijer et al., 2014), to date, CBZ has not been used to target other Nav isoforms based on their primary sequence.

Identification of gain-of-function mutations in Nav1.8 in individuals with painful peripheral neuropathy suggest that Nav1.8 channels contribute to neuropathic pain in peripheral neuropathy (Faber et al., 2012b; Han et al., 2014; Huang et al., 2013), and thus inhibitors of this

Mol #113076

channel may have therapeutic benefits. Whether the novel mode-of-action of CBZ extends to other Navs is not known. We describe here, in an individual with painful diabetic neuropathy a novel mutation in Nav1.8, S242T. Using patch-clamp recordings, we investigated the effects of the mutation at the channel level by voltage-clamp, and the effects of expressing mutant channels on the excitability of DRG neurons by current-clamp. We extrapolated from studies of CBZ interaction with the homologous Nav1.7-S241T mutation to ask whether the novel mechanism of action for this drug as activation modulator extends to Nav1.8-S242T, and to determine whether CBZ at clinically-achievable concentration reduces hyperexcitability of DRG neurons expressing the mutant channel. Our studies ultimately aim to determine whether the novel mode-of-action of CBZ is isoform-specific.

Mol #113076

Materials and Methods

Patient and clinical examinations

A 67-year-old male diabetic patient was recruited as part of the Pain in Neuropathy Study (PiNS) (Themistocleous et al., 2016), an observational cross-sectional multicenter study approved by the National Research Ethics Service of the UK (No.: 10/H0706/35). All participants signed informed consent, consent of PiNS participants (2010-2015) was made on the basis that they would not be told the result of the sequencing of voltage gated sodium channel genes. A detailed description of the study protocol is previously given (Themistocleous et al., 2016). Clinical assessment included clinical history, structured neurological examination, skin biopsy to determine the intra-epidermal nerve fiber density (IENFD) and Quantitative sensory testing (QST).

Pain intensity was reported on an 11-point numerical rating scale, with 0 being no pain and 10 the worst pain imaginable and pain location indicated on a body map. The Douleur Neuropathique 4 Questionnaire (DN4) (Bouhassira et al., 2005) was used as a screening tool for neuropathic pain. A comprehensive structured upper and lower limb neurological examination was performed to detect clinical signs of a peripheral neuropathy (Compston, 2010; Kleyweg et al., 1991). The examination included assessment of light touch, pinprick sensation, proprioception, vibration perception, deep-tendon reflexes, muscle bulk, and motor power. The clinical findings were quantified with the Toronto Clinical Scoring System (TCSS) (Bril and Perkins, 2002). TCSS is a screening tool for diabetic peripheral neuropathy and correlates with diabetic neuropathy severity.

The determination of IENFD followed the European Federation of Neurological Societies/Peripheral Nerve Society Guideline on the utilization of skin biopsy (Lauria et al.,

Mol #113076

2010). QST is a measure of sensory perception in response to a given stimulus and can be used to demonstrate abnormalities in sensory function. QST was performed over the dorsum of both feet, in line with the published protocol of the German research network of neuropathic pain (DFNS) (Rolke et al., 2006). Raw QST data was transformed into z-scores to normalize for age, sex, and the body location of testing (Maier et al., 2010; Rolke et al., 2006). A z-score of zero is equal to the mean of the population. A score of greater or less than two standard deviations from the mean indicates gain-of-function or loss-of-function, respectively. Additional drug, laboratory, and clinical investigation data were retrieved from the clinical medical records.

Sequencing of sodium channels

Sequencing of the coding regions of *SCN9A* (encodes Nav1.7), *SCN10A* (encodes Nav1.8) and *SCN11A* (encodes Nav1.9) was undertaken by next generation sequencing using the HaloPlex Target Enrichment System (Agilent Technologies, Santa Clara, CA, USA) and MiSeq Sequencing Platform (Illumina, Inc., San Diego, CA, USA) following DNA extraction from blood. Variants were called using an in-house bioinformatics pipeline (further details available on request). Any variant that was both (1) present at >1% allele frequency in the Exome Variant Database (<http://evs.gs.washington.edu/EVS>) or Exome Aggregation Consortium (ExAC, <http://exac.broadinstitute.org>), and (2) not previously reported in the literature in association with painful neuropathy was considered unlikely to be pathogenic and was not investigated further. Rare variants that were present at <1% allele frequency in population databases were considered for further analysis, irrespective of whether they were previously reported in the literature in association with painful neuropathy or not. Variants of potential interest were confirmed by Sanger sequencing by capillary electrophoresis using a 3730 DNA Analyzer (Applied

Mol #113076

Biosystems, Foster City, CA, USA). The *in silico* prediction of the functional effect of the variant was performed using multiple algorithms: Align GVGD (<http://agvgd.hci.utah.edu/>), SIFT (<http://sift.jcvi.org>) and Polyphen-2 (<http://genetics.bwh.harvard.edu/pph2/>).

Structural modeling

Homology models for both the Nav1.8 and Nav1.7 were developed based on the recently published electric eel sodium channel structure (Yan et al., 2017) by using the homology modeler tool in Molecular Operating Environment (MOE) software (*Molecular Operating Environment (MOE)*, 2013.08; Chemical Computing Group ULC, 1010 Sherbooke St. West, Suite #910, Montreal, QC, Canada, H3A 2R7, 2018).

Functional assessments of Nav1.8 S242T mutant

The *pcDNA5-GFP-2A-Nav1.8* plasmid encoding enhanced green fluorescent protein and a ‘StopGo’ 33 amino acid 2A linker upstream of the human Nav1.8 ATG codon was previously described (Faber et al., 2012b; Han et al., 2014; Huang et al., 2013). The nucleotide substitution c.724T>A, which leads to the amino acid substitution Ser242Thr was introduced into the construct using QuikChange® Lightning site-directed mutagenesis (Agilent, Santa Clara, CA, USA).

Primary mouse DRG neuron isolation and transfection

Animal studies were approved by United States Veterans Affairs West Haven medical center Animal Care and Use Committee. DRG neurons were isolated, as previously reported (Faber et al., 2012b; Han et al., 2014; Huang et al., 2013), from homozygous Nav1.8-cre mice (4–8 weeks

Mol #113076

of age, both male and female) that lack functional endogenous Nav1.8 channels. In compliance with recent NIH guidelines and our own practice, we have used both male and female mice as source for DRG neurons. Briefly, DRGs were harvested, incubated at 37°C for 20 min in complete saline solution (CSS) (in mM: 137 NaCl, 5.3 KCl, 1 MgCl₂, 25 sorbitol, 3 CaCl₂, and 10 N-2-hydroxyethylpiperazine-N'-2-ethanesulfonic acid (HEPES), adjusted to pH 7.2 with NaOH), containing 0.5 U/ml Liberase TM (Sigma-Aldrich, St. Louis, MO, USA) and 0.6 mM EDTA, followed by a 15min incubation at 37°C in CSS containing 0.5 U/ml Liberase TL (Sigma), 0.6 mM EDTA, and 30 U/ml papain (Worthington Biochemical, Lakewood NJ, USA). Tissue was then centrifuged and triturated in 0.5 ml of DRG media: Dulbecco's Modified Eagle Medium/F12 (1:1) with 100 U/ml penicillin, 0.1 mg/ml streptomycin (Life Technologies, Grand Island, NY, USA) and 10% fetal bovine serum (Hyclone, , Logan, UT, USA), containing 1.5 mg/ml bovine serum albumin (BSA) (low endotoxin; Sigma) and 1.5 mg/ml trypsin inhibitor (Sigma). After trituration, Nav1.8-WT or Nav1.8-S242T mutant channel constructs were transfected into DRG neurons in suspension using a Nucleofector IIS electroporator (Lonza, Walkersville, MD, USA) and Amaxa SCN Nucleofector reagents (VSP1-1003). After electroporation, 100 µl of calcium-free Dulbecco's modified Eagle medium (Lonza) was added and cells were incubated at 37°C for 5 min in a 95% air/5% CO₂ (vol/vol) incubator to allow neurons to recover. The cell mixture was then diluted with DRG media containing 1.5 mg/ml bovine serum albumin (low endotoxin; Sigma) and 1.5 mg/ml trypsin inhibitor (Sigma), seeded onto poly-D-lysine/laminin-coated coverslips (Corning, Discovery Labware, Bedford, MA, USA) and incubated at 37°C to allow DRG neurons to attach to the coverslips. After 40 min incubation, DRG media was added into each well to a final volume of 1.0 ml [for current-clamp recording culture, medium was supplemented with 50 ng/ml mouse nerve growth factor

Mol #113076

(Alomone Labs, Jerusalem, Israel) and 50 ng/ml recombinant human glial cell line-derived neurotrophic factor (PeproTech, Rocky Hill, NJ, USA) and the DRG neurons were maintained at 37°C in a 95% air/5% (vol/vol) CO₂ incubator for 40~48 h before recording.

Electrophysiology and pharmacology

Voltage-clamp and Current-clamp recordings were obtained with an EPC-10 amplifier (HEKA Electronics, Holliston, MA, USA) from small transfected mouse DRG neurons (<25µm diameter) with robust green fluorescence at room temperature (~22 °C), 40–48 h after transfection, as described previously (Faber et al., 2012b; Han et al., 2015; Han et al., 2014; Huang et al., 2013). As in our previous studies (Faber et al., 2012a), to minimize variability of DRG neuron cultures prepared at different times, we carried out head-to-head comparison of cells transfected with WT or mutant channels, and of cells treated with CBZ or vehicle, from cultures prepared contemporaneously by the same researcher.

Voltage-clamp recording from transfected Nav1.8-null mouse DRG neurons

Fire-polished electrodes (1–2MΩ) were fabricated from 1.6mm outer diameter borosilicate glass micropipettes (World Precision Instruments, Sarasota, FL, USA). The pipette potential was adjusted to zero before seal formation, and liquid junction potential was not corrected. Capacitive transients were cancelled and voltage errors were minimized with 80–90% series resistance compensation; cells were excluded from analysis if the predicted voltage error exceeded 4 mV. Leakage current was digitally subtracted on-line using hyperpolarizing control pulses, applied before the test pulse (P/6 subtraction). Currents were acquired with PatchMaster software (HEKA Electronics), 5 min after establishing whole-cell configuration, sampled at a

Mol #113076

rate of 50 kHz, and filtered at 2.9 kHz. The pipette solution contained the following (in mM): 140 CsF, 10 NaCl, 1 EGTA, and 10 HEPES, pH 7.3 with CsOH (adjusted to 315 mOsmol/L with dextrose). The extracellular bath solution contained the following (in mM): 70 NaCl, 70 choline chloride, 3 KCl, 1 MgCl₂, 1 CaCl₂, 10 HEPES, 5 CsCl, 20 tetraethylammonium chloride (TEA·Cl), pH 7.32 with NaOH (327mOsmol/L). TTX (0.5μM), CdCl₂ (0.1mM), and 4-aminopyridine (1mM) were added in the bath solution to block endogenous tetrodotoxin-sensitive (TTX-S) voltage-gated sodium currents, calcium currents, and potassium currents, respectively. Endogenous Nav1.9 currents were suppressed by holding the cells at -70 mV, a step which inactivates Nav1.9 channels and minimize their contribution to the TTX-R current (Cummins et al., 1999).

For current–voltage relationships, cells were held at -70 mV and stepped to a range of potentials (-70 to +40 mV in 5 mV increments) for 100 ms with the 5-s interval between each sweep. Peak inward currents (*I*) were plotted as a function of depolarization potential to generate *I*-*V* curves. Activation curves were obtained by converting *I* to conductance (*G*) at each voltage (*V*) using the equation $G=I/(V-V_{rev})$, where V_{rev} is the reversal potential which was determined for each cell individually. Each cell's activation curve was then fit with Boltzmann functions in the form of $G=G_{max}/(1+ \exp[(V_{1/2,act}-V)/k])$, where G_{max} is the maximal sodium conductance, $V_{1/2,act}$ is the potential at which activation is half-maximal, *V* is the test potential and *k* is the slope factor. The fit parameters such as activation $V_{1/2}$ are grouped and then evaluated for significance between groups using 2-tailed t-test.

Steady-state fast-inactivation was achieved with a series of 500 ms prepulses (-90 to +10 mV in 5 mV increments) and the remaining non-inactivated channels were activated by a 40 ms step depolarization to 0 mV. The protocol for slow-inactivation consisted of a 30s step to

Mol #113076

potentials varying from -120 to 20 mV, followed by a 30 ms step to -70 mV to remove fast-inactivation and a 20 ms step to 0 mV to elicit a test response. Peak inward currents obtained from steady-state fast-inactivation and slow-inactivation protocols were normalized by the maximum current amplitude for each cell and fit with a Boltzmann equation of the form $I/I_{max} = A + (1-A) / (1 + \exp[(V - V_{1/2,inact})/k])$, where V represents the inactivating prepulse potential, $V_{1/2,inact}$ represents the midpoint of the inactivation. The fit parameters such as inactivation $V_{1/2}$ are grouped and then evaluated for significance between groups using 2-tailed t-test.

Deactivation was estimated from current decay, using a 3 ms short depolarizing pulse to 0 mV followed by a 100 ms repolarizing pulse to potentials ranging from -110 to -20 mV in 5 mV increments, and the holding potential for deactivation was -70 mV. Deactivation kinetics were calculated by fitting the decaying currents with a single exponential function. Differences between groups are evaluated point-by-point using unpaired 2-tailed t-tests with Bonferroni's correction for multiple comparisons.

Persistent currents were measured as mean amplitudes of currents recorded between 85 and 95ms after the onset of depolarization and are presented as a percentage of the maximal transient peak current. Ramp currents were elicited with slow ramp depolarization over a 600-ms period at 0.2 mV/ms. The amplitude of ramp current was presented as a percentage of the maximal peak current. Differences between groups are evaluated point-by-point using unpaired 2-tailed t-tests with Bonferroni's correction for multiple comparisons.

Current-clamp recording from transfected Nav1.8-null mouse DRG neurons

In order to reduce observer bias, current-clamp recordings were performed in a blind manner where the electrophysiologist was not aware whether the neurons were transfected with wild-

Mol #113076

type or mutant channels. Electrodes had a resistance of 1-3 M Ω when filled with the pipette solution, which contained the following (in mM): 140 KCl, 0.5 EGTA, 5 HEPES, and 3 Mg-ATP, pH 7.3 with KOH (adjusted to 315 mosM with dextrose). The extracellular solution contained the following (in mM): 140 NaCl, 3 KCl, 2 MgCl₂, 2 CaCl₂, and 10 HEPES, pH 7.3 with NaOH (adjusted to 320 mosM with dextrose). Whole-cell configuration was obtained in voltage-clamp mode before proceeding to the current-clamp recording mode. Current threshold was determined by the first action potential elicited by a series of 200 ms depolarizing current injections that increased in 5 pA increments with the sweep interval of 10-s. Cells with stable resting membrane potentials more negative than -40 mV and overshooting action potentials (>80 mV resting membrane potential to peak) were used for additional data collection. Action potential frequency was determined by quantifying the number of action potentials elicited in response to depolarizing current injections (500-ms).

Carbamazepine treatment

Carbamazepine (CBZ) was purchased from Sigma (St. Louis, MO, USA), and a stock is prepared by dissolving in dimethylsulfonamide (DMSO). For pharmacology experiments, CBZ aliquots were added to produce a working solution of a clinically-achievable concentration of CBZ (30 μ M) (Breton et al., 2005) in 0.1% DMSO (final concentration). Cells were treated with CBZ (30 μ M), or 0.1% DMSO in incomplete DRG media (without the 10% FBS) for 30 min before recording and the CBZ or DMSO was maintained in the bath solution during the recording as described previously (Fischer et al., 2009; Geha et al., 2016; Yang et al., 2017; Yang et al., 2012). Shorter treatment periods of 2 and 5 minutes were not enough to produce depolarizing shift in activation of Nav1.7-S241T channels (data not shown), while a 30 min treatment period was

Mol #113076

effective and was thus implemented in the current studies, consistent with prior observations on the effect of CBZ on mutant Nav1.7 channels (Fischer et al., 2009; Geha et al., 2016).

Statistics

Voltage-clamp and current-clamp data were analyzed using FitMaster (HEKA Electronics), and OriginPro8.5 (OriginLab Corporation, Northampton, MA, USA). As described above, we carried out head-to-head comparison of cells transfected with WT or mutant channels, and of cells treated with CBZ or vehicle, from cultures prepared contemporaneously by the same researcher, to minimize culture-to-culture variability. Except where noted, statistical significance was determined using an independent 2-tailed *t* test with unequal variance, with Bonferroni's correction for multiple comparisons when appropriate. Percentages of spontaneously firing cells were compared using the *z* test. *Mann-Whitney* test was used to compare current threshold. The number of evoked action potentials between two different groups was evaluated using 2-way ANOVA. All electrophysiology data are presented as the mean \pm SEM, and error bars in the figures represent the SEM. A P value of less than 0.05 was considered statistically significant.

Mol #113076

Results

Case history

The 67-year-old male patient had been diagnosed with type-2 diabetes mellitus at the age of 42, and his recent HbA1C was 8.2 %. He developed pain, paresthesia, and numbness in both of his feet 12 years prior to assessment for this study. At the time of assessment, he reported pain and paresthesia in his feet and hands. He rated pain intensity over the 24 hours before clinical assessment as 3 out of 10, with a DN4 score of 7 (>4 indicative of neuropathic pain). He was not taking any analgesic medication. He did not complain of autonomic symptoms. His deceased father had also suffered from painful diabetic neuropathy but no further family members were available for segregation analysis.

Neurological examination identified a severe length-dependent sensory neuropathy that extended to his knees and wrists bilaterally with no weakness. Deep tendon reflexes were absent at the knees and ankles bilaterally. Toronto Clinical Scoring System (TCSS) score was 17, indicative of a severe neuropathy. Quantitative sensory testing (QST) revealed bilateral hyposensitivity in relation to both thermal and mechanical detection thresholds. The intraepidermal nerve fiber density (IENFD) assessed at 10 cm above the lateral malleolus was markedly reduced (0 fibers/mm). The clinical presentation was therefore of a severe painful sensory neuropathy in a patient with a longstanding history of type 2 diabetes mellitus. Because of the family history of painful sensory neuropathy we screened for gene variants in those genes encoding Navs which have previously been linked to painful sensory neuropathy: *SCN9a*, *SCN10a* and *SCN11a*.

Mol #113076

Molecular genetics and structural modeling

Generally, our interest is discovery of rare variants (<1%) as we are looking for variants that potentially have a high impact on channel function, recognizing that not every rare variant will have a large effect, and that there are a small number of relatively common variants which confer gain-of-function attributes on voltage gated sodium channels in the context of painful neuropathy (Waxman et al., 2014).

Sequencing of *SCN9A* and *SCN11A* genes, encoding for the Nav_v1.7 and Nav_v1.9 sodium channels, respectively, did not identify any pathogenic variants; there were no rare variants (<1%) in these channels or variants that had previously been linked to painful neuropathy. However, a potentially pathogenic variant (c.724T>A, rs140288103) was found in *SCN10A*, the gene that encodes Nav_v1.8. The c.724T>A missense variant changes the amino acid 242 of Nav_v1.8 channel from a serine to a threonine (S242T). The variant was present at a low frequency (MAF 0.0002) in both Exome Variant Database (EVS) and Exome Aggregation Consortium (ExAC) databases. Prediction programs Align GVGD, SIFT and PolyPhen-2 classified the substitution S242T as “C55, likely to interfere with function”, “deleterious” and “probably damaging”, respectively. S242 is located in the domain I S4-S5 linker of Nav_v1.8 and is invariant in the voltage-gated sodium channel family (Fig. 1A). A homologous mutation S241T in Nav_v1.7 has been previously reported in families with the pain disorder inherited erythromelalgia (IEM) in Europe (Michiels et al., 2005) and North America (Geha et al., 2016).

We implemented structural modeling based on the recently reported structure of eukaryotic sodium channel from electric eel (Yan et al., 2017) using the MOE program. The homology modeling was performed using MOE defaults. Since the eel structure published by Yan et al. (Yan et al., 2017) did not resolve the intracellular loops L1 (between DI and DII) and L2 (between DII and DIII), the corresponding amino acid sequences of hNav_v1.7 and hNav_v1.8

Mol #113076

were removed before performing the homology modeling (Fig. 1B). Our homology model shows that the location of the Nav1.8-S242T residue within the DI/S4-S5 linker and the orientation of the side chain matches exactly the Nav1.7-S241T residue (Fig. 1B), which suggests that the serine to threonine substitution in this linker confers similar physiological and pharmacological attributes on Nav1.8 as it does on Nav1.7.

Functional analysis of Nav1.8-S242T mutant channels

Voltage-clamp analysis

Voltage-clamp recordings were obtained from DRG neurons from Nav1.8-null mice transfected with Nav1.8-WT (referred to as WT) or Nav1.8-S242T (referred to as S242T) mutant channels. Fig. 2A shows representative human Nav1.8 sodium currents recorded from cells expressing WT channels, and Fig. 2B from cells expressing S242T mutant channels. The current density in cells expressing S242T channels was not different from that of WT channels (WT: 325 ± 49 pA/pF, $n=26$; S242T: 267 ± 30 pA/pF, $n=30$; $P = 0.315$, t-test). The midpoint of activation for S242T ($V_{1/2}$) was shifted by -6.1 mV to -17.82 ± 1.35 mV (95% CI: -20.58 mV, -15.05 mV, $n = 30$), compared with WT channels (-11.73 ± 0.97 mV, 95% CI: -13.74 mV, -9.73 mV, $n = 26$; $P = 0.0006$; t-test) (Fig. 2C). Kinetics of activation were investigated by measuring the time-to-peak of the transient current. Considering the observed shift in $V_{1/2}$ of activation induced by the S242T mutation, we expected faster activation depending on the step voltage. Activation of S242T channels from -40 mV to -10 mV was statistically significantly (2-tailed t test with Bonferroni's correction, *, $P < 0.05$) faster than that of WT channels (Fig. 2D). We also measured the kinetics of deactivation. As shown in Fig. 3E, the rates of current decay of S242T mutant channels were statistically significantly (2-tailed t test with Bonferroni's correction, *, $P < 0.05$) slower than

Mol #113076

those of WT channels at deactivation potentials from -30 mV to -10 mV.

The $V_{1/2}$ of fast-inactivation for S242T channels (-38.24 ± 1.08 mV, $n=25$) was hyperpolarized by 3.8 mV compared to that for WT channels (-34.47 ± 0.86 mV, $n=24$, $P=0.0088$, t-test) (Fig. 3F). As Fig. 3G shows, steady-state slow-inactivation of S242T channels was enhanced, compared to WT channels. The $V_{1/2}$ of S242T channels (-56.11 ± 1.21 mV, $n=13$) was hyperpolarized by 8.9 mV compared with that of WT channels ($V_{1/2}$: -47.20 ± 1.56 mV, $n=14$, $P=0.0001$, 2-tailed t-test).

We measured the response of WT and S242T channels to a slow ramp stimulus. The ramp current for S242T channels ($22.60\% \pm 1.45\%$ of peak current, $n=26$) was not different from that of WT channels ($22.54\% \pm 0.92\%$ of peak current, $n=25$; $P = 0.974$, 2-tailed t-test); however, the average voltage where the peak of ramp current occurs was shifted by -6.4 mV for S242T channels (-22.77 ± 1.44 mV, $n=26$) compared with that for WT channels (-16.34 ± 0.80 mV, $n=25$, $P=0.0004$, 2-tailed t-test) (Fig. 2H). Figure 2I compares the normalized amplitudes of persistent currents in DRG neurons expressing WT and S242T channels. The persistent currents of S242T channels were statistically significantly (2-tailed t test with Bonferroni's correction, *, $P<0.05$) larger than the persistent currents of WT channels over the voltage from -50 mV to -25 mV, whereas the S242T mutant channels produced smaller persistent currents than WT channels at more depolarized voltages between -10 mV to +20 mV.

Current-clamp analysis

We assessed the effect of the S242T mutant channels at the cellular level using current-clamp recordings on DRG neurons from Nav1.8-null mice transfected with either WT or S242T channels. The resting membrane potential of DRG neurons expressing S242T channels ($-55.6 \pm$

Mol #113076

1.4mV, n=29) was comparable to that of DRG neurons expressing WT channels (-54.9 ± 1.1 mV, n=31; $P = 0.728$, t-test). The input resistance of DRG neurons expressing S242T channels (362 ± 32 M Ω , n=29) was also comparable to that of DRG neurons expressing WT channels (319 ± 38 M Ω , n=31, $P = 0.391$, t-test).

Current threshold, the minimal stimulus required to produce a single all-or-none action potential, was reduced in DRG neurons expressing S242T mutant channels. Fig. 3A shows traces from a representative DRG neuron expressing WT channels. In response to ≤ 105 pA sub-threshold current injections, the neuron only generated small, graded membrane potential depolarization. The first all-or-none action potential required a stimulus of 110 pA (current threshold for this neuron). Figure 3B shows recordings from a representative DRG neuron which expressed S242T mutant channels. For this neuron, the current injection required to produce the first all-or-none action was 70 pA. Figure 3C presents a comparison of current threshold for a population of these two groups of neurons. The average threshold for DRG neurons expressing S242T mutant channels (64 ± 14 pA, n=29, 95% CI: 34 pA, 93pA) was smaller compared with that of neurons expressing WT channels (124 ± 21 pA, n=31, 95% CI: 81 pA, 166pA; $P = 0.0079$, Mann-Whitney test). There was no difference for action potential amplitude (WT: 110.4 ± 1.6 mV, n=31; S242T: 111.4 ± 1.9 mV, n=29, $P = 0.700$, t-test), or half-width of the action potential (WT: 8.28 ± 0.73 ms, n=31; S242T: 8.01 ± 0.58 ms, n=29, $P = 0.770$, t-test) between the two groups of DRG neurons.

The effect of WT and S242T channels on repetitive firing properties of DRG neurons was assessed by applying a series of 500 ms current injections to the two groups of DRG neurons. Representative action potentials triggered by increasing current injections of 150, 300, and 450 pA in neurons transfected with either WT or S242T channels are illustrated in Fig. 3D-I. Cells

Mol #113076

expressing S242T (Fig. 3G-I) fired with a higher frequency than cells expressing WT channels (Fig. 3D-F) in response to similar stimuli. The average numbers of action potentials in cells expressing WT or S242T elicited by graded current injections in 50 pA steps are plotted in Fig. 3J. Compared with neurons expressing WT channels, neurons expressing S242T channels produced higher firing frequencies at every stimulus level across the broad range studied, which reached statistical significance (2-way ANOVA: genotype x stimulus strength, $P < 0.001$). In addition, we observed that among both groups of DRG neurons, a subpopulation of neurons fired spontaneously. The proportion of spontaneously firing neurons for the group of DRG neurons expressing S242T channels (23 out of 52 cells, 44.2%) was not different from that of DRG neurons expressing WT channels (15 out of 46 cells, 32.6%; $P = 0.235$, two-portion z-test).

We would note that our recordings were made in DRG neurons transfected with WT or mutant Nav1.8 channels, and thus express these channels at higher than normal levels, which is why, as in our prior studies (Faber et al., 2012a; Faber et al., 2012b; Han et al., 2015; Han et al., 2014; Huang et al., 2013), we did a head-to-head comparison of the effects of the expression of these channels in these neurons. We consider the difference in the neuronal behavior as the indicator of increased excitability induced by mutant channels.

Responsiveness of Nav1.8-S242T mutant channels to Carbamazepine

Carbamazepine rescues the hyperpolarizing shift of activation of S242T mutant channels

We have previously shown that pretreatment of cells with a clinically-achievable concentration of CBZ (30 μ M) (Breton et al., 2005) for 30 minutes depolarizes voltage-dependence of activation of Nav1.7 channels that carry the S241T substitution (Yang et al., 2012), at the analogous position to the S242T in Nav1.8 (Fig. 1A). Since the homology structure model shows

Mol #113076

that the spatial location of the Nav1.8-S242T residue corresponds with that of the Nav1.7-S241T residue (Fig. 1B), we hypothesized that Nav1.8-S242T might also be CBZ-responsive. To test this hypothesis, DRG neurons expressing S242T mutant channels were pretreated with DMSO or 30 μ M CBZ for 30 minutes before the recordings. Figures 4A and 4B show representative traces recorded from DRG neurons expressing S242T mutant channels after treatment with DMSO or CBZ, respectively. As Fig. 4C shows, CBZ treatment caused a depolarizing shift of 6.8 mV in the $V_{1/2}$ of voltage-dependence of activation of S242T mutant channels compared with DMSO treatment (DMSO: -18.00 ± 2.14 mV, $n=12$, 95% CI: -22.72 mV, -13.29 mV; CBZ: -11.19 ± 1.80 mV, $n=17$, 95% CI: -15.00 mV, -7.39 mV; $P = 0.023$, t-test). Treatment of DRG neurons with 30 μ M CBZ did not shift steady-state fast-inactivation of S242T mutant channels (Fig. 4D). The $V_{1/2}$ of steady-state fast-inactivation for CBZ treatment (-38.20 ± 2.93 mV, $n=11$) was not different from that for DMSO treatment (-37.54 ± 2.86 mV, $n=7$; $P = 0.875$, t-test). Treatment with 30 μ M CBZ also did not cause a statistically significant shift in the steady-state slow-inactivation of S242T mutant channels. The $V_{1/2}$ of steady-state slow-inactivation after DMSO treatment and CBZ treatment were -50.84 ± 1.59 mV ($n=13$) and -56.14 ± 3.11 mV ($n=11$; $P = 0.150$, t-test), respectively.

Carbamazepine does not shift activation of Nav1.8-WT channels

To determine whether carbamazepine treatment shifts activation of Nav1.8-WT channels, we incubated DRG neurons expressing WT channels with 30 μ M CBZ or DMSO. Fig. 5A and 5B show representative traces recorded from DRG neurons expressing WT channels after being treated with DMSO or CBZ, respectively. CBZ treatment did not shift voltage-dependence of activation of WT channels ($V_{1/2}$ of activation: DMSO: -13.49 ± 2.13 mV, $n=10$; CBZ: -11.44 ± 1.64

Mol #113076

mV, $n=14$; $P = 0.454$, 2-tailed t-test) (Fig. 5C). Treatment with 30 μM CBZ did not shift steady-state fast-inactivation of WT channels (Fig. 5D) ($V_{1/2}$ of fast-inactivation: DMSO: -36.26 ± 2.36 mV, $n=10$; CBZ: -36.84 ± 2.05 mV, $n=14$, $P = 0.855$, t-test), or steady-state slow-inactivation ($V_{1/2}$ of steady-state slow-inactivation: DMSO: -46.04 ± 2.12 mV, $n=13$; CBZ: -46.74 ± 1.56 mV, $n=13$, $P = 0.793$, 2-tailed t-test).

Carbamazepine reduces excitability of DRG neurons expressing Nav1.8-S242T mutant channels

As shown above, expression of Nav1.8-S242T mutant channels increased the excitability of DRG neurons. Because pretreatment with CBZ depolarized activation of S242T mutant channels, shifting their $V_{1/2}$ of activation to a voltage close to that of WT channels (Fig. 4C), we hypothesized that pretreatment with CBZ should attenuate the increased excitability of DRG neurons expressing S242T mutant channels. Current-clamp recording was implemented to evaluate the effect of CBZ pretreatment on the excitability of DRG neurons expressing S242T mutant channels.

Pretreatment of transfected DRG neurons with 30 μM CBZ for 30 min did not alter the resting membrane potential of DRG neurons expressing S242T channels compared to the DMSO control (DMSO: -52.0 ± 1.1 mV, $n=28$; CBZ: -54.5 ± 0.8 mV, $n=29$; $P = 0.078$, 2-tailed t-test). Input resistance of DRG neurons expressing S242T channels was not different between cells treated with CBZ (315 ± 55 M Ω , $n=29$) or DMSO (366 ± 62 M Ω , $n=28$; $P = 0.545$, 2-tailed t-test). Figure 6A shows traces of a representative neuron expressing S242T mutant channels treated with DMSO. Current threshold for this neuron was 55 pA. In contrast, Fig. 6B shows traces of a representative neuron expressing S242T mutant channels treated with CBZ, and the current

Mol #113076

threshold for this neuron was 90 pA. On average, CBZ treatment doubled the current threshold for DRG neurons expressing S242T mutant channel (DMSO: 55 ± 8 pA, $n=28$, 95% CI: 39 pA, 71 pA; CBZ: 114 ± 21 pA, $n=29$, $P=0.012$, 95% CI: 71 pA, 157 pA; $P = 0.037$, Mann-Whitney test, Fig. 6C). However, there was no difference in action potential amplitude between the CBZ and DMSO treated neurons (DMSO: 104.5 ± 1.8 mV, $n=28$; CBZ: 106.4 ± 1.5 mV, $n=29$; $P = 0.417$, t-test). The half-width of action potential was also not different between the two groups of DRG neurons (DMSO: 8.33 ± 0.83 mV, $n=28$; CBZ: 9.78 ± 1.25 mV, $n=29$; $P = 0.338$, 2-tailed t-test).

We further investigated the effect of CBZ treatment on the firing frequency of DRG neurons expressing S242T mutant channels. As shown in Fig. 6D-F, a neuron treated with DMSO produced multiple action potentials in response to 500 ms depolarizing current steps of 150 pA, 300 pA and 450 pA. In contrast, a neuron treated with CBZ (Fig. 6G-I) generated fewer action potentials in response to same current injections. Compared with the treatment with DMSO, the treatment with CBZ caused a marked reduction in the firing frequencies for DRG neurons expressing S242T mutant channels which reached statistical significance (2-way ANOVA: treatment x stimulus strength, $P < 0.001$) (Fig. 6J). Although we observed a reduction in the proportion of spontaneously firing neurons treated with CBZ (DMSO: 45.1%, 23 out 51 cells; CBZ: 35.1%, 16 out 45 cells), this difference did not reach statistical significance ($P = 0.315$, two-portion z -test). This data shows that CBZ treatment attenuated the hyperexcitability of DRG neurons expressing S242T mutant channels.

Carbamazepine does not cause reduction in the excitability of DRG neurons expressing Nav1.8-WT channels

We evaluated whether treatment with 30 μ M CBZ for 30 min attenuates the excitability of DRG

Mol #113076

neurons expressing Nav1.8-WT channels. Figures 7A and 7B show traces of two representative neurons expressing WT channels after treatment with DMSO or 30 μ M CBZ, respectively. Current threshold for these two neurons were 155 pA (DMSO, Fig. 7A) and 135 pA (CBZ, Fig. 7B). On average, the current threshold for DRG neurons expressing WT channels after treatment with CBZ (137 ± 23 pA, $n=27$) was not different from that of neurons treated with DMSO (132 ± 24 pA, $n=25$; $P = 0.912$, Mann-Whitney test) (Fig. 7C). We also found that treatment with CBZ had no effects on resting membrane potential (DMSO: -54.8 ± 1.4 mV, $n=25$; CBZ: -55.1 ± 1.3 mV, $n=27$; $P = 0.875$, t-test), input resistance (DMSO: 313 ± 43 M Ω , $n=25$; CBZ: 264 ± 41 M Ω , $n=27$), amplitude (DMSO: 105.7 ± 1.5 mV, $n=25$; CBZ: 107.8 ± 1.2 mV, $n=27$; $P = 0.277$, t-test) and half-width (DMSO: 9.51 ± 1.07 ms, $n=25$; CBZ: 9.55 ± 1.11 ms, $n=27$; $P = 0.977$, t-test) of action potentials.

We compared the firing frequency of DRG neurons expressing WT channels after treatment with CBZ or DMSO. Fig. 7D-I shows responses of two representative DRG neurons expressing WT channels after treatment of DMSO (Fig. 7D-F) or CBZ (Fig. 7G-I). Both neurons produced the same or nearly the same number of spikes in response to 150, 300 or 450 pA current injection. As summarized in Fig. 7J, across the range of current stimuli we studied, treatment of CBZ resulted in a small but statistically significant difference in the firing frequency of DRG neurons expressing WT channels compared to treatment with DMSO (2-way ANOVA: treatment x stimulus strength, $P < 0.05$). In addition, compared with DMSO treatment, CBZ treatment did not change the proportion of spontaneously firing neurons (DMSO: 13 out 38 cells, 34.2%; CBZ: 11 out 38 cells, 28.9%; $P=0.619$, two-portion z-test).

Mol #113076

Discussion

We report here the novel Nav1.8-S242T mutation in a patient with neuropathic pain and DPN. Voltage-clamp recordings in DRG neurons show that S242T confers a complex phenotype at the channel level, manifesting both gain-of-function attributes including a hyperpolarizing shift of activation, and loss-of-function attributes including a hyperpolarizing shift in slow-inactivation. Current-clamp recordings demonstrated that S242T mutant channels render DRG neurons hyperexcitable, indicating a dominant role for the gain-of-function attributes, consistent with neuropathic pain in this patient. We previously showed (Yang et al., 2012) that the homologous S241T mutation in Nav1.7 endows this channel with a unique mode of responsiveness to CBZ: depolarization of voltage-dependence of activation. We demonstrate here that CBZ depolarizes voltage-dependence of activation of Nav1.8-S242T mutant channel and reduces excitability of DRG neurons expressing these channels. These data suggest that the novel activity of CBZ as an activation modulator extends from Nav1.7 to Nav1.8.

The presence of this mutation could not be assessed in the deceased father, preventing analysis of genetic segregation. Nevertheless, our data suggest that S242T might be “pathogenic” or “probably pathogenic” based on criteria that have been established for analysis of variants in voltage-gated sodium channels (Waxman et al., 2014). The variant was absent in the cohort of diabetic patients without pain and is exceedingly rare in the genomic databases (MAF 0.0002). *In silico* analysis identified S242T as damaging and deleterious. The S242T mutation occurs at a position in the DI/S4-5 linker where a homologous gain-of-function mutation in Nav1.7 which causes IEM (Geha et al., 2016; Lampert et al., 2006; Michiels et al., 2005). As shown in this study, functional assessment of S242T shows that it confers gain-of-function attributes on Nav1.8 and renders DRG neurons hyperexcitable. One possible explanation for the late-onset of

Mol #113076

symptoms is that altered metabolic milieu secondary to diabetes, for example elevated methylglyoxal, which has been previously shown to depolarize Nav1.8 inactivation (Bierhaus et al., 2012) further enhancing gain-of-function attributes of the mutant channel, may have been required for full manifestation of clinical symptoms. However, this is a small study with genetic and clinical data available for only one patient and given the fact that DPN is potentially a gene-environment interaction, large cohorts will be needed for replication and to establish pathogenicity.

The Nav1.8-S242T substitution within the Domain I/S4-S5 linker is homologous to the Nav1.7-S241T mutation, identified in subjects with IEM (Geha et al., 2016; Michiels et al., 2005). Homology modeling based on the CryoEM structure of the electric eel sodium channel (Yan et al., 2017) shows a conserved position and orientation of the S/T substitution in Nav1.7 and Nav1.8. The S4-5 linker transduces the movement of the voltage-sensor into a conformational change in the pore module during opening of the activation gate (Payandeh et al., 2011), which suggests that activation properties of the Nav1.8 mutant channel would be altered by this substitution. Indeed, voltage-clamp recordings showed that, similar to the effect of the S241T substitution on Nav1.7, Nav1.8-S242T channel activation is hyperpolarized and accelerated, and deactivation is slowed, all gain-of-function features. However, unlike the Nav1.7-S241T channels, Nav1.8-S242T channels displayed enhanced fast- and slow-inactivation, both loss-of-function features. Enhanced fast-inactivation has not been previously reported for mutations of the S4-5 linkers in Nav1.7-S241T or Nav1.7-I234T; however, the Nav1.7-I234T mutation in the S4-5 linker manifests massive enhancement of slow-inactivation by about -20 mV (Ahn et al., 2010). Local structural alterations due to intra-molecular interactions of the S/T substitution or altered interactions of the threonine mutant residue with

Mol #113076

phospholipids in the plasma membrane might produce channel isoform-specific effects on gating.

Because the S242T mutation confers both gain-of-function (hyperpolarized and accelerated activation and slower deactivation) and loss-of-function (enhanced fast- and slow-inactivation) biophysical attributes on Nav1.8 it was not possible to predict *a priori* whether it would increase neuronal excitability. Current-clamp analysis showed that the Nav1.8-S242T channels rendered DRG neurons hyperexcitable, manifested as reduced current threshold and increased evoked firing. It is well-established that DRG neurons sit at resting potentials in the -50 to -60 mV range (Faber et al., 2012a; Faber et al., 2012b; Fang et al., 2006; Hendrich et al., 2012), and a hyperpolarizing shift in activation of Nav1.8 and increase in persistent current close to the resting potential of these neurons would be expected to increase excitability (Huang et al., 2018). Hyperpolarized and accelerated activation and increased persistent currents at relatively hyperpolarized potentials of Nav1.8-S242T compared to WT channels would be expected to increase excitability of DRG neurons. The increased excitability of DRG neurons that we observed (Fig. 4) is consistent with the pain reported by the patient carrying the Nav1.8-S242T mutation.

Building upon the observation that CBZ depolarizes voltage-dependence of activation of Nav1.7-S241T channels (Yang et al., 2012) and attenuates excitability of DRG neurons expressing these channels (Geha et al., 2016), we reasoned that the S242T mutation in Nav1.8, which corresponds to S241T in Nav1.7, would be CBZ-responsive. Our data show that clinically-achievable concentration of CBZ (30 μ M) also depolarizes the voltage-dependence of activation of Nav1.8-S242T channels (Fig. 4C) and attenuates firing of DRG neurons expressing the mutant channel (Fig. 6). By contrast, similar treatment with CBZ of DRG neurons expressing

Mol #113076

WT Nav1.8 channels did not depolarize the voltage-dependence of activation of the channel (Fig. 5) and only slightly reduced firing of DRG neurons (Fig. 7). Although a CBZ concentration of 30 μ M could act on other sodium channels, our data suggest that attenuation of firing of neurons expressing the mutant channel is more likely due to the effect of CBZ as an activation modifier. This conclusion is supported by the observation that CBZ pre-treatment of DRG neurons that expressed the Nav1.7-F1449V mutant channels, whose activation is not modified by CBZ, did not attenuate firing of these neurons (Yang et al., 2012).

The normalizing effect of CBZ on activation of Nav1.7 mutant channels I234T, S241T, and V400M (Fischer et al., 2009; Geha et al., 2016; Yang et al., 2017; Yang et al., 2012) is novel, and has not been previously reported for drugs that bind at the Nav channels local anesthetic (LA) binding site. This effect is also distinct from classical state-dependent blocking of Nav channels in that it requires pre-treatment with CBZ (Fischer et al., 2009; Geha et al., 2016; Yang et al., 2017; Yang et al., 2012). Whether this novel-mode-of action of CBZ on Nav1.7 and Nav1.8 mutations is due to formation of a new binding site is not known. The fact that DI/S4-5 S/T substitution in both channels responded to CBZ in the same manner, however, suggests a common mechanism, despite differences in the primary sequence of the two channels even within the highly conserved linker sequence (Fig. 1A). Elucidation of the molecular determinants of productive drug-target interactions in channels other than Nav1.7 might be useful in establishing molecular and structural requirements for this novel mode-of-action of CBZ.

A recent systematic review found that the evidence for efficacy of CBZ in neuropathic pain treatment was inconclusive and noted dose-limiting side effects (Finnerup et al., 2015). CBZ is not therefore used as a first line treatment for neuropathic pain (first line treatments include GABA-pentinoids, tricyclic anti-depressants and serotonin-noradrenaline reuptake inhibitors);

Mol #113076

however, CBZ is still used clinically in selected patients with some success, especially because of its demonstrable effectiveness in patients with trigeminal neuralgia (Maarbjerg et al., 2017). It is increasingly clear that there are multiple pathophysiological drivers of neuropathic pain and we need to find better ways of stratifying patients in order to aid treatment selection (Themistocleous et al., 2018). A recent study reported that patients with a specific pattern of sensory dysfunction termed the irritable nociceptor (defined by mechanical hypersensitivity and preserved small fibre function on QST) had a better treatment response to oxcarbazepine compared to those without this feature (Demant et al., 2014). A further approach to patient stratification is to use molecular genetics. Recently, patients with S241T and I234T were shown to respond to CBZ treatment which was predicted using an approach which employed atomic-level structure modeling, mutant cycle analysis and *in vitro* pharmacological testing (Geha et al., 2016; Yang et al., 2017; Yang et al., 2012). Thus far, it has been unclear if this precision medicine approach can be extended to mutations in other sodium channels. Although we could not test the efficacy of CBZ in this subject due to limitations imposed by the approved protocol, our current-clamp recordings demonstrate that 30 μ M CBZ attenuates Nav1.8-S242T induced hyperexcitability of DRG neurons, suggesting that CBZ treatment might be beneficial for individuals carrying this mutation.

In summary, we have described a novel gain-of-function Nav1.8 mutation in a patient with diabetes and neuropathic pain. Nav1.8-S242T mutant channels manifest dominant gain-of-function attributes and render DRG neurons hyperexcitable. Exposure to clinically-achievable concentration of CBZ corrects the mutation-induced hyperpolarized shift of voltage-dependence of activation and attenuates the hyperexcitability of DRG neurons expressing Nav1.8-S242T channels. Our data suggest that the novel mode-of-action of CBZ can be extended from Nav1.7

Mol #113076

to Nav1.8, and more generally suggest that the precision medicine approach capitalizing on this finding might produce beneficial outcomes to individuals carrying CBZ-responsive Nav1.8 mutations.

Mol #113076

Acknowledgements: We thank Palak Shah and Dr. Peng Zhao for technical assistance. We also thank Dr. Daria Sizova, Dr. Yang Yang, Dr. Brian Tanaka, Dr. Jianying Huang and Dr. Malgorzata Mis for valuable comments.

Authorship Contributions:

Participated in Research Design: S. Dib-Hajj, Bennett and Waxman

Conducted Experiments: Han, Themistocleous, Estacion, Blesneac and Fratter

Contributed new reagents or analytical tools: F. Dib-Hajj and Macala

Performed data analysis: Han, Themistocleous, Estacion, Blesneac, Fratter, Bennett, Waxman and S. Dib-Hajj

Wrote or contributed to the writing of the manuscript: Han, Themistocleous, Estacion, Bennett, Waxman and S. Dib-Hajj

The authors declare no conflict of interest

Mol #113076

References

- Ahn HS, Dib-Hajj SD, Cox JJ, Tyrrell L, Elmslie FV, Clarke AA, Drenth JP, Woods CG and Waxman SG (2010) A new Na_v1.7 sodium channel mutation I234T in a child with severe pain. *Eur J Pain* **14**(9): 944-950.
- Akopian AN, Sivilotti L and Wood JN (1996) A tetrodotoxin-resistant voltage-gated sodium channel expressed by sensory neurons. *Nature* **379**(6562): 257-262.
- Ambrosio AF, Soares-Da-Silva P, Carvalho CM and Carvalho AP (2002) Mechanisms of action of carbamazepine and its derivatives, oxcarbazepine, BIA 2-093, and BIA 2-024. *Neurochem Res* **27**(1-2): 121-130.
- Bennett DL and Woods CG (2014) Painful and painless channelopathies. *Lancet Neurol* **13**(6): 587-599.
- Bierhaus A, Fleming T, Stoyanov S, Leffler A, Babes A, Neacsu C, Sauer SK, Eberhardt M, Schnolzer M, Lasischka F, Neuhuber WL, Kichko TI, Konrade I, Elvert R, Mier W, Pirags V, Lukic IK, Morcos M, Dehmer T, Rabbani N, Thornalley PJ, Edelstein D, Nau C, Forbes J, Humpert PM, Schwaninger M, Ziegler D, Stern DM, Cooper ME, Haberkorn U, Brownlee M, Reeh PW and Nawroth PP (2012) Methylglyoxal modification of Na_v1.8 facilitates nociceptive neuron firing and causes hyperalgesia in diabetic neuropathy. *Nat Med* **18**(6): 926-933.
- Blair NT and Bean BP (2002) Roles of tetrodotoxin (TTX)-sensitive Na⁺ current, TTX-resistant Na⁺ current, and Ca²⁺ current in the action potentials of nociceptive sensory neurons. *J Neurosci* **22**(23): 10277-10290.
- Bouhassira D, Attal N, Alchaar H, Boureau F, Brochet B, Bruxelle J, Cunin G, Fermanian J, Ginies P, Grun-Overdyking A, Jafari-Schluep H, Lanteri-Minet M, Laurent B, Mick G, Serrie A, Valade D and Vicaut E (2005) Comparison of pain syndromes associated with nervous or somatic lesions and development of a new neuropathic pain diagnostic questionnaire (DN4). *Pain* **114**(1-2): 29-36.
- Breton H, Cociglio M, Bressolle F, Peyriere H, Blayac JP and Hillaire-Buys D (2005) Liquid chromatography-electrospray mass spectrometry determination of carbamazepine, oxcarbazepine and eight of their metabolites in human plasma. *J Chromatogr B Analyt Technol Biomed Life Sci* **828**(1-2): 80-90.
- Bril V and Perkins BA (2002) Validation of the Toronto Clinical Scoring System for diabetic polyneuropathy. *Diabetes Care* **25**(11): 2048-2052.
- Compston A (2010) Aids to the investigation of peripheral nerve injuries. Medical Research Council: Nerve Injuries Research Committee. His Majesty's Stationery Office: 1942; pp. 48 (iii) and 74 figures and 7 diagrams; with aids to the examination of the peripheral nervous system. By Michael O'Brien for the Guarantors of Brain. Saunders Elsevier: 2010; pp. [8] 64 and 94 Figures. *Brain* **133**(10): 2838-2844.
- Cummins TR, Dib-Hajj SD, Black JA, Akopian AN, Wood JN and Waxman SG (1999) A novel persistent tetrodotoxin-resistant sodium current in SNS-null and wild-type small primary sensory neurons. *J Neurosci* **19**(24): RC43.
- Demant DT, Lund K, Vollert J, Maier C, Segerdahl M, Finnerup NB, Jensen TS and Sindrup SH (2014) The effect of oxcarbazepine in peripheral neuropathic pain depends on pain phenotype: a randomised, double-blind, placebo-controlled phenotype-stratified study. *Pain* **155**(11): 2263-2273.
- Dib-Hajj SD, Black JA and Waxman SG (2015) NaV1.9: a sodium channel linked to human

Mol #113076

pain. *Nat Rev Neurosci* **16**(9): 511-519.

Dib-Hajj SD, Cummins TR, Black JA and Waxman SG (2010) Sodium Channels in Normal and Pathological Pain. *Annu Rev Neurosci* **33**: 325-347.

Dib-Hajj SD, Geha P and Waxman SG (2017) Sodium channels in pain disorders: pathophysiology and prospects for treatment. *Pain* **158 Suppl 1**: S97-S107.

Faber CG, Hoeijmakers JG, Ahn HS, Cheng X, Han C, Choi JS, Estacion M, Lauria G, Vanhoutte EK, Gerrits MM, Dib-Hajj S, Drenth JP, Waxman SG and Merkies IS (2012a) Gain of function Nav1.7 mutations in idiopathic small fiber neuropathy. *Ann Neurol* **71**(1): 26-39.

Faber CG, Lauria G, Merkies IS, Cheng X, Han C, Ahn HS, Persson AK, Hoeijmakers JG, Gerrits MM, Pierro T, Lombardi R, Kapetis D, Dib-Hajj SD and Waxman SG (2012b) Gain-of-function Nav1.8 mutations in painful neuropathy. *Proc Natl Acad Sci U S A* **109**(47): 19444-19449.

Fang X, Djouhri L, McMullan S, Berry C, Waxman SG, Okuse K and Lawson SN (2006) Intense isolectin-B4 binding in rat dorsal root ganglion neurons distinguishes C-fiber nociceptors with broad action potentials and high Nav1.9 expression. *J Neurosci* **26**(27): 7281-7292.

Fertleman CR, Baker MD, Parker KA, Moffatt S, Elmslie FV, Abrahamsen B, Ostman J, Klugbauer N, Wood JN, Gardiner RM and Rees M (2006) SCN9A mutations in paroxysmal extreme pain disorder: allelic variants underlie distinct channel defects and phenotypes. *Neuron* **52**(5): 767-774.

Finnerup NB, Attal N, Haroutounian S, McNicol E, Baron R, Dworkin RH, Gilron I, Haanpaa M, Hansson P, Jensen TS, Kamerman PR, Lund K, Moore A, Raja SN, Rice AS, Rowbotham M, Sena E, Siddall P, Smith BH and Wallace M (2015) Pharmacotherapy for neuropathic pain in adults: a systematic review and meta-analysis. *Lancet Neurol* **14**(2): 162-173.

Fischer TZ, Gilmore ES, Estacion M, Eastman E, Taylor S, Melanson M, Dib-Hajj SD and Waxman SG (2009) A novel Nav1.7 mutation producing carbamazepine-responsive erythromelalgia. *Ann Neurol* **65**(6): 733-741.

Geha P, Yang Y, Estacion M, Schulman BR, Tokuno H, Apkarian AV, Dib-Hajj SD and Waxman SG (2016) Pharmacotherapy for Pain in a Family With Inherited Erythromelalgia Guided by Genomic Analysis and Functional Profiling. *JAMA Neurol* **73**(6): 659-667.

Han C, Estacion M, Huang J, Vasylyev DV, Zhao P, Dib-Hajj S and Waxman SG (2015) Human Nav1.8: enhanced persistent and ramp currents contribute to distinct firing properties of human DRG neurons. *J Neurophysiol* **113**(9): 3172-3185.

Han C, Vasylyev D, Macala LJ, Gerrits MM, Hoeijmakers JG, Bekelaar KJ, Dib-Hajj SD, Faber CG, Merkies IS and Waxman SG (2014) The G1662S Nav1.8 mutation in small fibre neuropathy: impaired inactivation underlying DRG neuron hyperexcitability. *Journal of neurology, neurosurgery, and psychiatry* **85**((5)): 499-505.

Hendrich J, Alvarez P, Joseph EK, Ferrari LF, Chen X and Levine JD (2012) In vivo and in vitro comparison of female and male nociceptors. *J Pain* **13**(12): 1224-1231.

Hong S, Morrow TJ, Paulson PE, Isom LL and Wiley JW (2004) Early painful diabetic neuropathy is associated with differential changes in tetrodotoxin-sensitive and -resistant sodium channels in dorsal root ganglion neurons in the rat. *J Biol Chem* **279**(28): 29341-29350.

Huang J, Mis MA, Tanaka B, Adi T, Estacion M, Liu S, Walker S, Dib-Hajj SD and Waxman

Mol #113076

- SG (2018) Atypical changes in DRG neuron excitability and complex pain phenotype associated with a Nav1.7 mutation that massively hyperpolarizes activation. *Sci Rep* **8**(1): 1811.
- Huang J, Yang Y, Zhao P, Gerrits MM, Hoeijmakers JG, Bekelaar K, Merkies IS, Faber CG, Dib-Hajj SD and Waxman SG (2013) Small-Fiber Neuropathy Nav1.8 Mutation Shifts Activation to Hyperpolarized Potentials and Increases Excitability of Dorsal Root Ganglion Neurons. *J Neurosci* **33**(35): 14087-14097.
- Kleyweg RP, van der Meche FG and Schmitz PI (1991) Interobserver agreement in the assessment of muscle strength and functional abilities in Guillain-Barre syndrome. *Muscle Nerve* **14**(11): 1103-1109.
- Kuo CC (1998) A common anticonvulsant binding site for phenytoin, carbamazepine, and lamotrigine in neuronal Na⁺ channels. *Mol Pharmacol* **54**(4): 712-721.
- Kuo CC, Chen RS, Lu L and Chen RC (1997) Carbamazepine inhibition of neuronal Na⁺ currents: quantitative distinction from phenytoin and possible therapeutic implications. *Mol Pharmacol* **51**(6): 1077-1083.
- Lampert A, Dib-Hajj SD, Tyrrell L and Waxman SG (2006) Size matters: Erythromelalgia mutation S241T in Nav1.7 alters channel gating. *J Biol Chem* **281** (47): 36029-36035.
- Lauria G, Hsieh ST, Johansson O, Kennedy WR, Leger JM, Mellgren SI, Nolano M, Merkies IS, Polydefkis M, Smith AG, Sommer C and Valls-Sole J (2010) European Federation of Neurological Societies/Peripheral Nerve Society Guideline on the use of skin biopsy in the diagnosis of small fiber neuropathy. Report of a joint task force of the European Federation of Neurological Societies and the Peripheral Nerve Society. *Eur J Neurol* **17**(7): 903-912, e944-909.
- Maarbjerg S, Di Stefano G, Bendtsen L and Cruccu G (2017) Trigeminal neuralgia - diagnosis and treatment. *Cephalalgia*: 333102416687280.
- Maier C, Baron R, Tolle TR, Binder A, Birbaumer N, Birklein F, Gierthmuhlen J, Flor H, Geber C, Hugel V, Krumova EK, Landwehrmeyer GB, Magerl W, Maihofner C, Richter H, Rolke R, Scherens A, Schwarz A, Sommer C, Tronnier V, Uceyler N, Valet M, Wasner G and Treede RD (2010) Quantitative sensory testing in the German Research Network on Neuropathic Pain (DFNS): somatosensory abnormalities in 1236 patients with different neuropathic pain syndromes. *Pain* **150**(3): 439-450.
- Meijer IA, Vanasse M, Nizard S, Robitaille Y and Rossignol E (2014) An atypical case of SCN9A mutation presenting with global motor delay and a severe pain disorder. *Muscle Nerve* **49**(1): 134-138.
- Mert T and Gunes Y (2012) Antinociceptive activities of lidocaine and the Nav1.8 blocker A803467 in diabetic rats. *J Am Assoc Lab Anim Sci* **51**(5): 579-585.
- Michiels JJ, te Morsche RH, Jansen JB and Drenth JP (2005) Autosomal dominant erythromelalgia associated with a novel mutation in the voltage-gated sodium channel alpha subunit Nav1.7. *Arch Neurol* **62**(10): 1587-1590.
- Payandeh J, Scheuer T, Zheng N and Catterall WA (2011) The crystal structure of a voltage-gated sodium channel. *Nature* **475**(7356): 353-358.
- Renganathan M, Cummins TR and Waxman SG (2001) Contribution of Nav1.8 sodium channels to action potential electrogenesis in DRG neurons. *J Neurophysiol* **86**(2): 629-640.
- Rolke R, Baron R, Maier C, Tolle TR, Treede RD, Beyer A, Binder A, Birbaumer N, Birklein F, Botefur IC, Braune S, Flor H, Hugel V, Klug R, Landwehrmeyer GB, Magerl W, Maihofner C, Rolko C, Schaub C, Scherens A, Sprenger T, Valet M and Wasserka B (2006) Quantitative

Mol #113076

sensory testing in the German Research Network on Neuropathic Pain (DFNS): standardized protocol and reference values. *Pain* **123**(3): 231-243.

Tanelian DL and Brose WG (1991) Neuropathic pain can be relieved by drugs that are use-dependent sodium channel blockers: lidocaine, carbamazepine, and mexiletine.

Anesthesiology **74**(5): 949-951.

Themistocleous AC, Crombez G, Baskozos G and DL B (2018) Using stratified medicine to understand, diagnose and treat neuropathic pain. *Pain* **159** Suppl 1:S31-S42.

Themistocleous AC, Ramirez JD, Shillo PR, Lees JG, Selvarajah D, Orengo C, Tesfaye S, Rice AS and Bennett DL (2016) The Pain in Neuropathy Study (PiNS): a cross-sectional observational study determining the somatosensory phenotype of painful and painless diabetic neuropathy. *Pain* **157**(5): 1132-1145.

Waxman SG, Merkies IS, Gerrits MM, Dib-Hajj SD, Lauria G, Cox JJ, Wood JN, Woods CG, Drenth JP and Faber CG (2014) Sodium channel genes in pain-related disorders: phenotype-genotype associations and recommendations for clinical use. *Lancet Neurol* **13**(11): 1152-1160.

Yan Z, Zhou Q, Wang L, Wu J, Zhao Y, Huang G, Peng W, Shen H, Lei J and Yan N (2017) Structure of the Nav1.4-beta1 Complex from Electric Eel. *Cell* **170**(3): 470-482 e411.

Yang Y, Adi T, Effraim P, Chen L, Dib-Hajj SD and Waxman SG (2017) Reverse pharmacogenomics: carbamazepine normalizes activation and attenuates thermal-induced hyperexcitability of sensory neurons due to Nav1.7 mutation I234T. *Br J Pharmacol* **175**(12): 2261-2271.

Yang Y, Dib-Hajj SD, Zhang J, Zhang Y, Tyrrell L, Estacion M and Waxman SG (2012) Structural modelling and mutant cycle analysis predict pharmacoresponsiveness of a Nav1.7 mutant channel. *Nat Commun* **3**: 1186.

Yang YC, Huang CS and Kuo CC (2010) Lidocaine, carbamazepine, and imipramine have partially overlapping binding sites and additive inhibitory effect on neuronal Na⁺ channels. *Anesthesiology* **113**(1): 160-174.

Mol #113076

Funding

SDD-H and SGW were supported by Center Grant [B9253-C] from the Rehabilitation Research Service, Department of Veterans Affairs, USA, and a gift from The Erythromelalgia Association. DLB is a Wellcome Senior Clinical Scientist [202747/Z/16/Z}. DLB, IB and AT are members of the DOLORisk consortium funded by the European Commission Horizon 2020 [ID633491]. DLB and AT are members of the International Diabetic Neuropathy Consortium, the Novo Nordisk Foundation, grant [NNF14SA0006]. The Center for Neuroscience & Regeneration Research is a Collaboration of the Paralyzed Veterans of America with Yale University.

Reprint requests:

Sulayman D. Dib-Hajj, PhD

The Center for Neuroscience and Regeneration Research

VA Connecticut Healthcare System

950 Campbell Avenue, Bldg. 34

West Haven, CT 06516

Tel: (203)937-3802

Fax: (203)937-3801

E-mail: Sulayman.dib-hajj@yale.edu

Mol #113076

Figure Legends

Figure 1. (A) Sequence alignment and position of mutation in DI S4-S5 linker in Nav1.8 channel. The sequence of the DI S4-S5 linker is invariant in the 9 sodium channels from human. The substitution of Nav1.8-S242T is highlighted in red type, and the substitution of Nav1.7-S241T is highlighted in blue type. **(B)** Structural modeling of human Nav1.8 and human Nav1.7 channels. The two channel structures were superimposed and the membrane spanning segments showed good alignment. Domain 1 is colored blue in Nav1.8, and red in Nav1.7. The overall structure is tilted and rotated to give a clearer view of the domain I S4-S5 linker where the Nav1.8-S242T and Nav1.7-S241T substitution occurs. A box is drawn to indicate the region of the structure that is zoomed out to better show the Nav1.8-T242 residue (blue carbons) and Nav1.7-T241 residue (red carbons). The serine to threonine substitution in the domain I S4-S5 linker in Nav1.7 and Nav1.8 maintains the same position and orientation of the side chain.

Figure 2. Voltage-clamp analysis of Nav1.8/S242T mutant channels. **A & B,** Representative current traces recorded from Nav1.8-null DRG neurons expressing Nav1.8-WT (**A**) or Nav1.8-S242T (**B**) channels. **C,** Point-to-point curve of mean conductance of WT and S242T channels which shows that activation $V_{1/2}$ of Nav1.8-S242T (n=30) channels is hyperpolarized by 6.1 mV compared with Nav1.8-WT (n=26) channels (2-tailed *t* test, $P = 0.0006$). **D,** Point-to-point curve for mean time-to-peak shows that mutant Nav1.8-S242T channels (n=29) opens faster than Nav1.8-WT (n=25) at voltages from -40 mV to -10 mV (2-tailed *t* test with Bonferroni's correction, *, $P < 0.05$). **E,** Nav1.8-S242T (n=24) channels deactivate significantly slower than Nav1.8-WT (n=21) channels at the voltage from -30 mV to -20 mV (2-tailed *t* test with Bonferroni's correction *, $P < 0.05$). **F,** Compared with Nav1.8-WT (n=24), Nav1.8-S242T

Mol #113076

mutation (n=25) shifts $V_{1/2}$ for fast-inactivation by -3.8 mV in a hyperpolarized direction. **G**, Compared with Nav1.8-WT (n=14), Nav1.8-S242T mutation (n=13) enhances steady-state slow-inactivation with the $V_{1/2}$ shifting by -8.9 mV. **H**, Representative ramp currents for Nav1.8-WT and Nav1.8-S242T mutant. Compared with Nav1.8-WT (n=25) channels, Nav1.8-S242T (n=16) shifts the voltage at which the peak of ramp current occurs. **I**, Comparison of persistent currents between cells expressing Nav1.8-WT (n=26) channels and cells expressing Nav1.8-S242T (n=30) mutant channels for activation depolarization step pulses from -70 to 20 mV. (2-tailed t test with Bonferroni's correction *, $P < 0.05$)

Figure 3. Current-clamp analysis of effects of Nav1.8-S242T mutant channels on DRG neuron excitability. **A & B**, Representative action potential (AP) traces recorded from DRG neuron expressing Nav1.8-WT (**A**) or Nav1.8-S242T mutant (**B**) channels. Action potentials were elicited by 200-ms step depolarizing current injections from resting membrane potential. **C**, Comparison of current threshold for DRG neurons expressing Nav1.8-WT (n=31) and Nav1.8-S242T (n=29) mutant channels. Expression of Nav1.8-S242T channels reduces current threshold significantly. 2-tailed t -Test *, $P < 0.05$. **D-I**, Responses of a representative DRG neuron expressing Nav1.8-WT channels (**D-F**) or Nav1.8-S242T mutant channels (**G-I**) to 500-ms depolarization current steps that are 150 pA (left), 300 pA (middle) and 450 pA (right). **J**, Comparison of responses (number of impulses evoked by a 500-ms stimulus) for the populations of DRG neurons expressing Nav1.8-WT (n=29) or Nav1.8-S242T (n=24) channels across a range of step current injections from 50–500 pA. (2-way ANOVA ***, $P < 0.001$).

Mol #113076

Figure 4. Clinically-relevant concentration of CBZ rescued the hyperpolarizing shift on activation of Nav_v1.8-S242T mutant channels. **A & B**, Representative traces of current families recorded from DRG neurons expressing Nav_v1.8-S242T mutant channel treated with DMSO (**A**), or with 30 μM CBZ (**B**). **C**, Treatment with CBZ (n=17) significantly shifted the voltage-dependence of activation of Nav_v1.8-S242T mutant channel compared with the treatment with DMSO (n=12), 2-tailed t-Test *, P<0.05. **D**, Treatment with 30 μM CBZ (n=11) did not affect the voltage-dependence of steady-state fast-inactivation compared with the treatment with DMSO (n=7).

Figure 5. Clinically-relevant concentration of CBZ had no effect on Nav_v1.8-WT channels. **A & B**, Representative traces of current families recorded from DRG neurons expressing Nav_v1.8-WT channels treated with DMSO (**A**), or with 30 μM CBZ (**B**). **C**, Treatment with CBZ (n=14) did not shift the voltage-dependence of activation of Nav_v1.8-WT channels compared with treatment with DMSO (n=10). **D**, Treatment with 30 μM CBZ (n=14) did not affect the voltage-dependence of steady-state fast-inactivation compared with the treatment with DMSO (n=10).

Figure 6. Current-clamp analysis of the effects of CBZ treatment on DRG neurons expressing Nav_v1.8-S242T mutant channels. **A & B**, Representative action potential (AP) traces recorded from DRG neuron expressing Nav_v1.8-S242T mutant channels after the treatment of DMSO (**A**) or 30 μM CBZ (**B**). **C**, Comparison of current threshold for DRG neurons expressing Nav_v1.8-S242T mutant channels after the treatment of CBZ (n=29) or the treatment with DMSO (n=28) control. CBZ treatment increased current threshold significantly. 2-tailed t-Test *, P<0.05. **D-I**, Responses of a representative DRG neurons expressing S242T mutant channels after the

Mol #113076

treatment with DMSO (**D-F**) or CBZ (**G-I**) to 500-ms depolarization current steps that are 150 pA (left), 300 pA (middle) and 450 pA (right). **J**, Comparison of responses (number of impulses evoked by a 500-ms stimulus) in the population of DRG neurons expressing Nav1.8-S242T mutant channels with the treatment with CBZ (n=26) or treatment with DMSO (n=23) control across a range of step current injections from 50–500 pA. 2-way ANOVA ***, P<0.001.

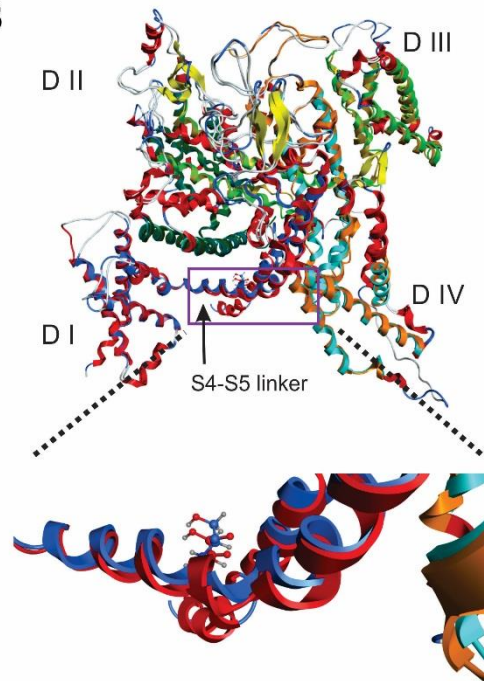
Figure 7. Current-clamp analysis of the effects of CBZ treatment on DRG neurons expressing Nav1.8-WT channels. **A & B**, Representative action potential (AP) traces recorded from DRG neuron expressing Nav1.8-WT channels after treatment of DMSO (**A**) or 30 μ M CBZ (**B**). **C**, Comparison of current threshold for DRG neurons expressing Nav1.8-WT channels after treatment of CBZ (n=27) or DMSO (n=25) control. CBZ treatment did not have significant effect on current threshold. **D-I**, Responses of the representative DRG neurons expressing Nav1.8-WT channels after treatment with DMSO (**D-F**) or CBZ (**G-I**) to 500-ms depolarization current steps that are 150 pA (left), 300 pA (middle) and 450 pA (right). **J**, Comparison of responses (number of impulses evoked by a 500-ms stimulus) in the population of DRG neurons expressing Nav1.8-WT channels with the treatment with CBZ (n=25) or DMSO (n=20) control across a range of step current injections from 50–500 pA, 2-way ANOVA *, P<0.05.

Mol #113076

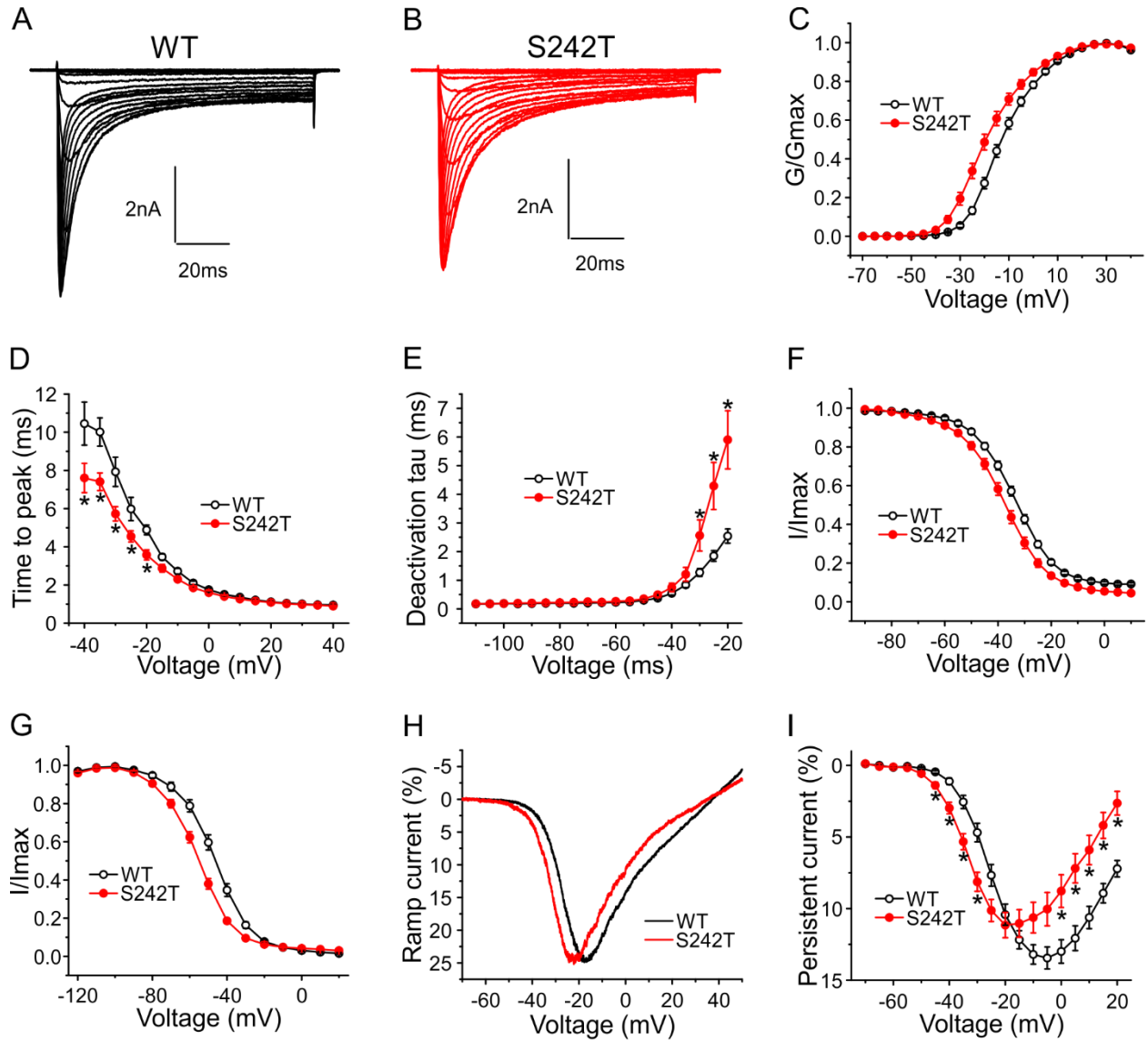
A

Nav1.1	KTIVGALIQSVKKLSD
Nav1.2	KTIVGALIQSVKKLSD
Nav1.3	KTIVGALIQSVKKLSD
Nav1.4	KTIVGALIQSVKKLSD
Nav1.5	KTIVGALIQSVKKLAD
Nav1.6	KTIVGALIQSVKKLSD
Nav1.7	KTIVGALIQSVKKLSD
Nav1.8	KVIVGALIH ^S VKKLAD
Nav1.9	KVIVGALLRSVKKLVN
Nav1.7 ^{S241T}	KTIVGALIQ ^T VKKLSD
Nav1.8 ^{S242T}	KVIVGALIH ^T VKKLAD

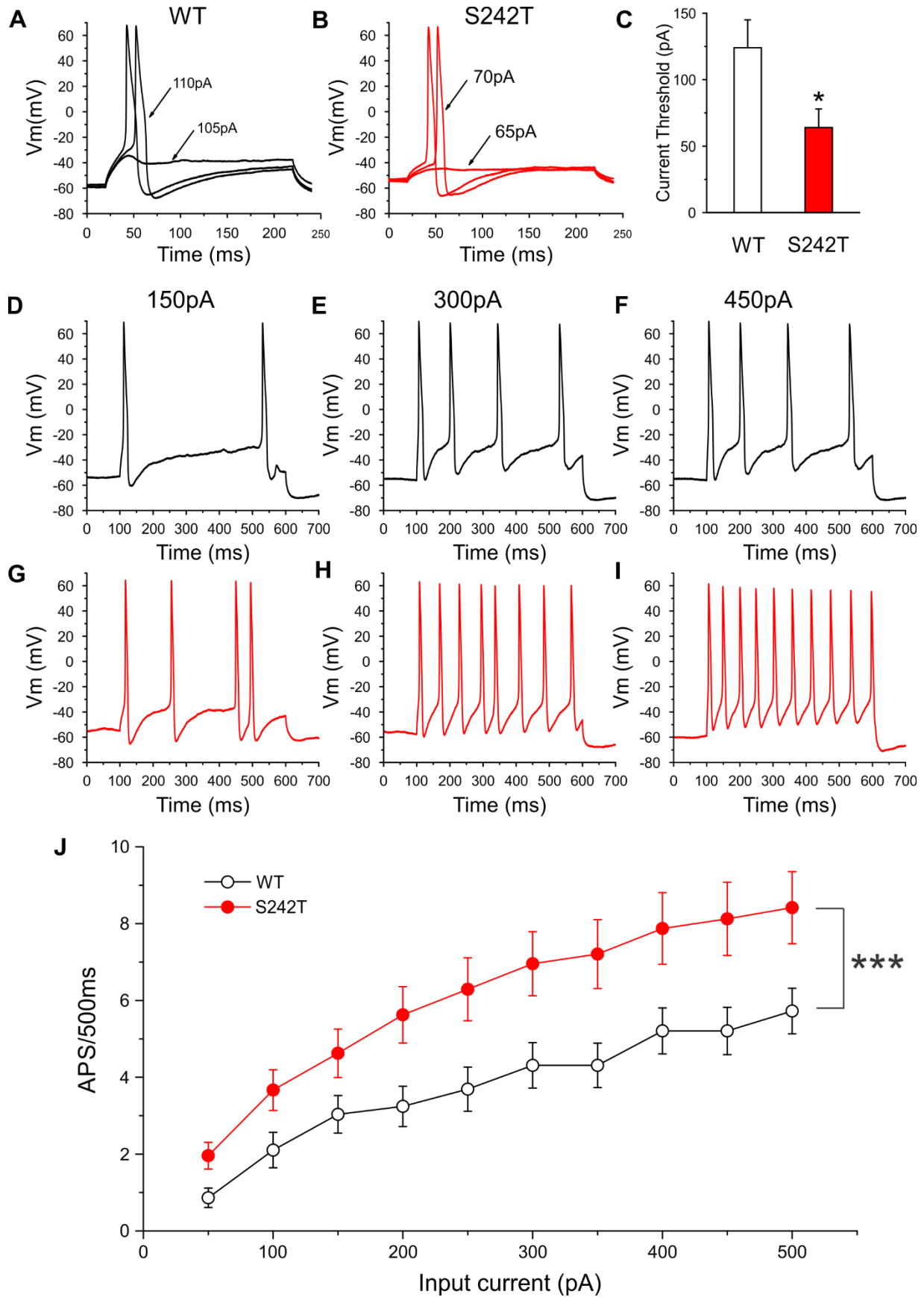
B



Mol #113076



Mol #113076



Mol #113076

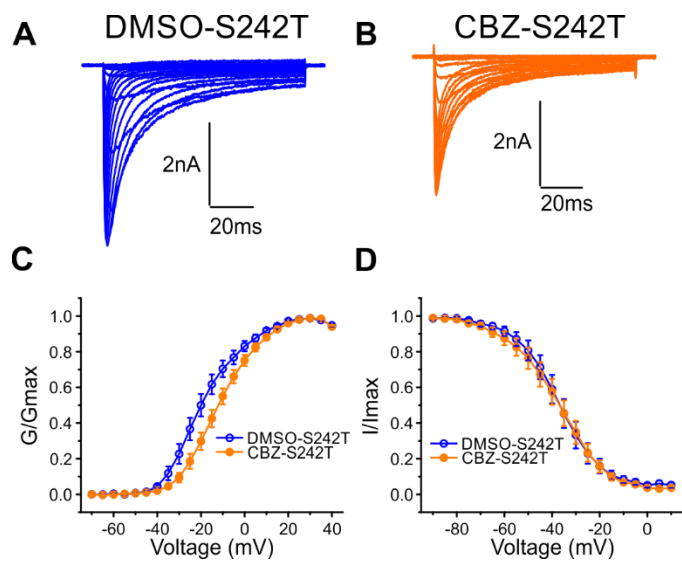


Figure 4

Mol #113076

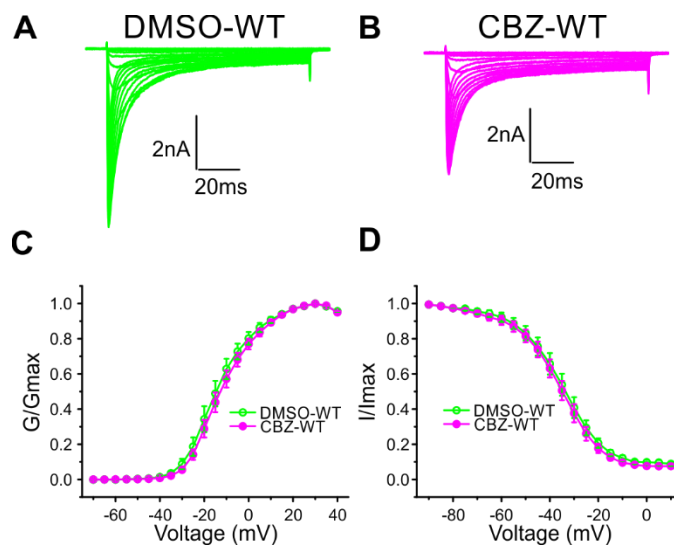
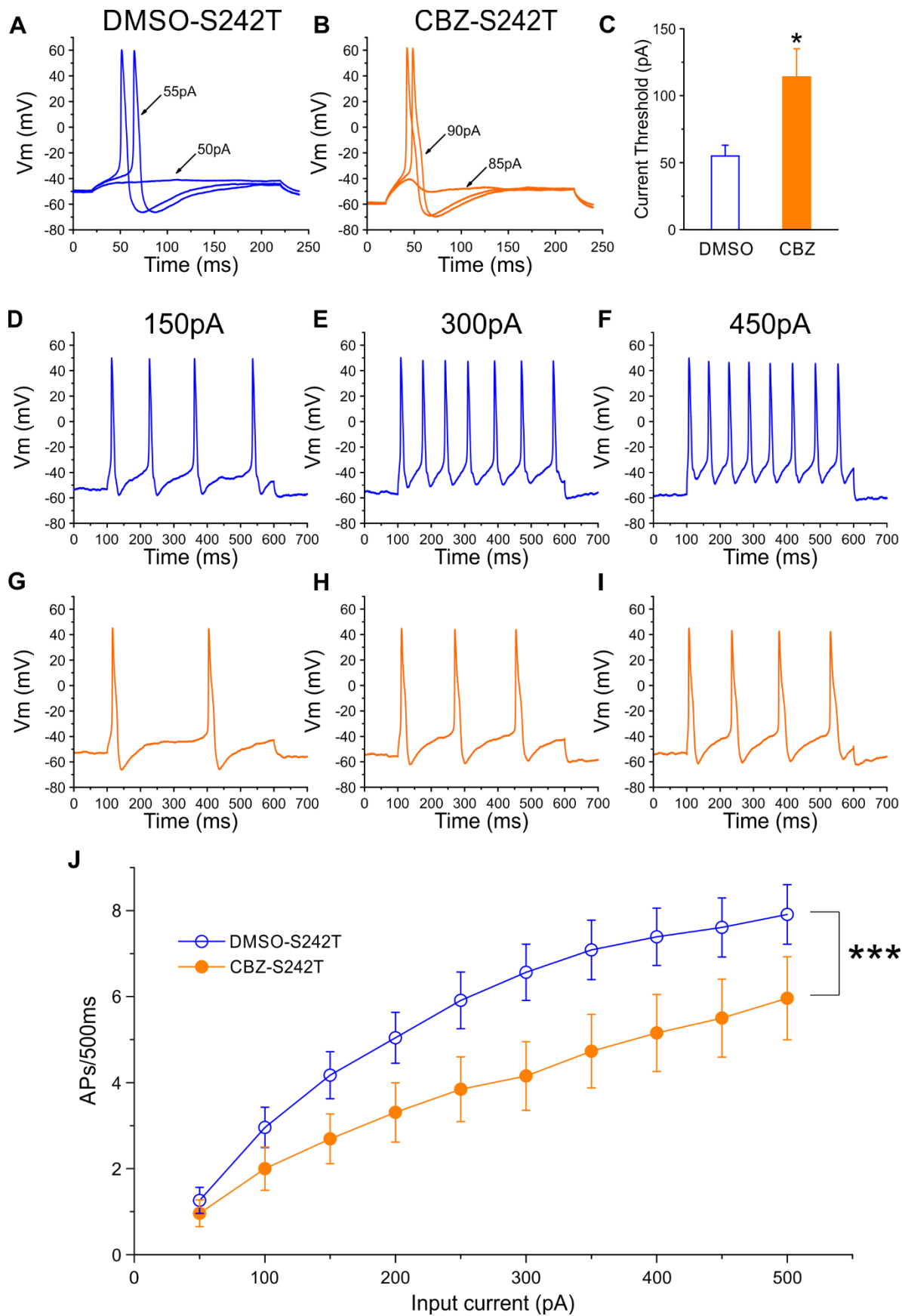


Figure 5

Mol #113076



Mol #113076

